https://doi.org/10.1016/j.compstruct.2018.10.004

# Joining of carbon fiber and aluminum using ultrasonic additive manufacturing (UAM)

Hongqi Guo[a], M. Bryant Gingerich[a], Leon M. Headings[a], Ryan Hahnlen[b], Marcelo J. Dapino[a,*]

[a]*Department of Mechanical and Aerospace Engineering, The Ohio State University, 201 W 19th Ave, Columbus, OH, 43210, USA*
[b]*Honda R&D Americas Inc, 21001 State Route 739, Raymond, OH 43067, USA*

**Abstract**

Various methods have been reported to join carbon fiber reinforced polymer (CFRP) composites with aluminum alloy (AA), with strengths ranging from 13 MPa to 112 MPa. This paper presents a new method for joining carbon fiber composites and metals using ultrasonic additive manufacturing (UAM). Although UAM is a metal 3D printing process, it is applied here to produce continuous CF-AA transition joints that can have uniform thickness across the CF and AA constituents. Joint strength is achieved by mechanical interlocking of CF loops within the AA matrix; tensile tests demonstrate that UAM CFRP-AA joints reach strengths of 129.5 MPa. The dry CF fabric extending from these joints can be laid up and cured into a CFRP part, whereas the AA can be welded to metal structures using traditional metal welding techniques – hence their designation as "transition joints." This approach enables the incorporation of CFRP parts into structures without requiring modifications to existing metal welding infrastructure. Two failure modes, CF tow failure and AA failure, have been identified. It is shown that the joint failure mode can be designed for maximum strength or maximum energy dissipation by adjusting the ratio of embedded CF to AA matrix.

*Keywords:* Ultrasonic additive manufacturing, CFRP joining, Hybrid structure, Aluminum alloy

## 1. Introduction

Structural lighweighting is critical for achieving improved vehicle fuel economy. A national energy study conducted by the US Department of Energy [1, 2] estimates that a 10% reduction in vehicle mass can lead to 6% reduction in fuel consumption. Due to their high specific strength and high specific stiffness, composites are commonly used in aerospace structures; their use in automotive applications is expected to increase. High-strength organic fibers such as CF or Zylon reach specific strengths that are an order of magnitude greater than typical automotive structural metals [3]. However, low specific toughness, high cost of materials, and complex process requirements make CFRP ill-suited for

*Corresponding author
*Email address:* dapino.1@osu.edu (Marcelo J. Dapino)

high-volume automotive manufacturing. Hybrid, multi-material structures that combine the beneficial characteristics of CFRP composites and typical automotive metals are therefore attractive. Methods to reliably join CFRP components to metallic structural components are thus required. The approach proposed in this paper consists of using the ultrasonic additive manufacturing (UAM) process to add metal tabs to a CFRP structure, and thus enable joining of the CFRP structure and a metal body via conventional resistance spot welding (RSW). Being able to incorporate CFRP structures into mass-production vehicles without requiring changes to existing metal welding infrastructure would save the automotive industry from making large investments in equipment and training.

CFRP has been joined with metal using adhesives, which presents limitations including long curing time, weak peel strength, and degradation due to aging [4]. Arenas et al. [5] investigated different structural adhesives with various surface pre-treatments for CFRP-AA joints. Considering both the mechanical performance and the industrial feasibility, it was found that using a polyurethane adhesive with a peel ply CFRP surface and a sanded AA surface is the best option, which can generate a joint with a lap shear strength of 12.42 MPa. Ribeiro et al. [6] used adhesive XNR6852 to join CFRP with AA and obtained a strength of 21 MPa. Alternatively, mechanical fasteners can be used for dissimilar material joining. However, fasteners can compromise fatigue life and disrupt the continuity of the joint. Additionally, they are often expensive and require time-consuming drilling processes. The strengths and weaknesses of mechanical joints have been studied by Marannano et al. [7] via double-lap CFRP-AA joints. It was shown that a higher mechanical strength can be obtained by adding steel rivets to CFRP and AA 6082-T6 adhesive joints. However, the riveting process induces delamination in the CFRP around the rivets. Lambiase et al. [8] applied a two-step clinching process and generated a CFRP-AA joint with a 6.6 mm diameter clinching area. Tensile tests showed that the lap shear joint carries a peak load of 2.3 kN. Zhai et al. [9] investigated the strength of countersunk CFRP-AA bolted joints and obtained a lap shear strength of 500 MPa (based on the bearing area).

Several innovative welding techniques have been presented for joining CFRP to metals. Balle et al. [10] applied the ultrasonic metal spot welding process to join CFRP to metal sheets. The lap shear strength of a joint between AA 5754 and carbon fiber reinforced Polyamide 66 (PA66) was shown to reach 31.5 MPa. Lionetto et al. [11] modified this joining method by adding a Polyamide 6 (PA6) film on top of the CFRP part before welding. With this modification, the lap shear strength increased to 34.8 MPa. Friction lap joining was proposed by Nagatsuka et al. [12] to directly join CFRP with AA 5052. This method generates joints with a magnesium oxide layer at the interface, and produces a joint strength of 2.9 kN for a 225 $mm^2$ weld area. Andre et al. [13] applied friction spot joining (FSpJ) with a polyphenylene sulfide (PPS) film interlayer to join AA 2024 with a CF-PPS composite. The average lap shear strength of this modified FSpJ joint reaches 52 MPa. Goushegir et al. [14] used a FSpJ method to join a 2 mm thick AA 2024-T3 sheet with a 2 mm thick CF-PPS composite.

With phosphoric acid anodizing and primer applied on the aluminum surface before welding, a lap shear peak load of 8788 N was obtained with a nugget diameter of approximately 10 mm. Mitschang et al. [15] reported that a lap shear strength of 14.5 MPa can be obtained by using induction spot welding to join AA 5754 to CF-PA66. Zajkani et al. [16] applied an electromagnetic forming process for CFRP-AA joining and obtained a lap shear force of over 1700 N for a 7.7 mm diameter circular joint region. A key limitation of these joining methods is the reliance on the strength of the epoxy adhesive to transfer all of the applied load from the fiber to the metal.

## 2. CFRP-AA joint using ultrasonic additive manufacturing

The joining approach presented in this paper employs ultrasonic additive manufacturing (UAM), a solid-state welding technology that incorporates ultrasonic metal welding in a continuous process to build 3D parts from foil stock [17]. The UAM process is illustrated in Figure 1. Two piezoelectric transducers vibrate the sonotrode parallel to the welding surface at 20 kHz and an operator-specified amplitude. A metal foil is fed under the textured sonotrode, which applies a normal force and vibrates the foil relative to the base material. The normal and shear forces at the weld interface collapse asperities and disperse oxides. This creates intimate metal-to-metal contact which results in solid-state welding between the foil and substrate.

The ultrasonic welder is built into a CNC milling station which also enables subtractive machining operations. After a desired number of layers are welded, material can be removed by installed milling tools. Channels with complex geometries can be machined to house non-metallic materials that can then be encapsulated by welding more foils over the channels. In the UAM process, local temperatures at the weld interface stay below 30% to 50% of the melting temperature of the foil stock [18]. This characteristic makes UAM a suitable method to embed a variety of materials including temperature sensitive materials and sensors. Hahnlen et al. [19, 20] used UAM to embed thermally-sensitive shape memory NiTi fibers into aluminum, which has the effect of reducing the coefficient of thermal expansion of the composite relative to aluminum. Although no metallurgical bonding was shown between the NiTi and AA matrix, interfacial strength arising from friction coupling was demonstrated using pullout tests and finite element analysis [21]. Delicate sensors such as Fiber Bragg Grating (FBG) can also be embedded into an aluminum matrix via UAM [22]. The UAM technology is not only able to weld thin foils, but can also weld thick aluminum sheets as demonstrated by Wolcott et al. [23] in a study on seam welding between 1.93 mm thick aluminum sheets.

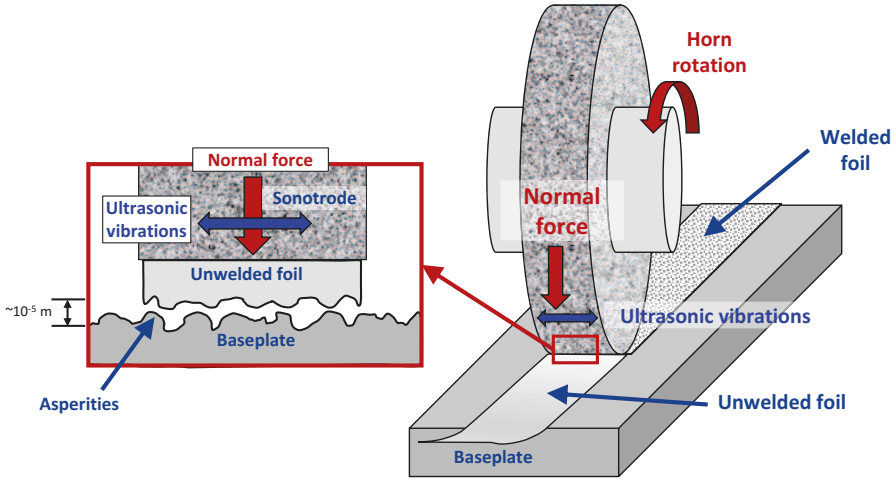


Figure 1: Ultrasonic additive manufacturing process (schematic not to scale). The normal force and lateral vibrations collapse asperities and disperse oxides to produce intimate metal-to-metal contact, resulting in solid-state welding.

In this study, UAM is used to embed dry CF fabric within AA; a key characteristic of our approach is that the CF-AA UAM joints are created before layup and curing of the CF within a CFRP composite structure. In contrast, most other CFRP-AA joining methods connect a cured CFRP laminate to a metal structure. Our joint design avoids the damage to the CFRP associated with drilling holes for fasteners and is able to create a strong mechanical connection between the dissimilar materials. Mechanical interlocking of CF loops in the AA matrix, facilitated by the UAM process, provides direct load transfer. This is in contrast to conventional joining methods where epoxy is a primary load-carrying component of the joint. Rather than creating a traditional joint with overlapping CFRP and metal regions, UAM makes it possible to create joints with a uniform thickness across the CFRP and AA constituents. To illustrate, a CFRP-AA demonstration part has been made (Figure 2). Aluminum flanges were joined to the dry CF via UAM, followed by the creation of the CFRP beam (using standard CFRP processes), and subsequent welding to an aluminum plate via conventional resistive spot welding. This paper describes the manufacturing process that enables the creation of UAM CF-AA transition joints (Section 3). Optical imaging and mechanical testing of cured CFRP-AA transition joints are presented which illustrate the mechanical properties of the joints (Sections 4 and 5, respectively). Tensile tests elucidate that two different failure modes are possible, leading the way to joints that can be designed for maximum mechanical strength or maximum energy dissipation, as summarized in Section 6.

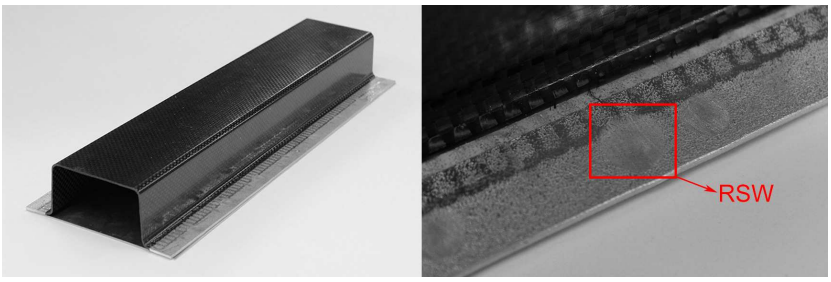


Figure 2: Example hybrid CFRP-metal hat structure with UAM transition joints and RSW welds to connect the AA transition to a flat metal sheet (at the bottom of the hat).

## 3. Experimental methods

### *3.1. Materials and components*

The CFRP component includes bidirectionally woven 3K carbon fiber fabric tape supplied by Fibre Glast Developments Corp. In this carbon fiber product, a single CF tow is woven from side-to-side, forming the weft and producing loops along the sides. The CFRP laminate is prepared with System 2000 epoxy paired with System 2120 hardener. Both the epoxy and the hardener are supplied by Fibre Glast Developments Corp. The resin and hardener are mixed at a ratio of 1:0.27. After applying the mixture to CF fabrics, the laminate is vacuum bagged and cured at room temperature. The experimental ultimate tensile strength (UTS) of each constituent material of the CFRP-AA joint sample is listed in Table 1. The UTS of the CFRP tow was measured by testing a single carbon fiber tow cured with epoxy; the area used for the CFRP tow strength calculation is based on a 7 $\mu$m fiber diameter (from SEM measurements) and the voids or epoxy among the fibers are not accounted for in the strength calculation. AA 6061-H18 foil is used as the feedstock for the UAM process. This is an annealed ASM standard AA 6061 material that has been fully work hardened [17]. The foil has a thickness of 0.152 mm and width of 25.4 mm. Foils are welded as-received, with no cleaning or pre-treatment applied. The UTS for UAM welded AA 6061 was measured by tensile tests of dogbone samples.

Table 1: Experimentally measured ultimate tensile strengths of CFRP-AA joint materials.

| | Ultimate tensile strength |
|---|---|
| CFRP component | 587 MPa |
| CFRP tow | 1.73 GPa |
| UAM welded AA 6061 | 195 MPa |

*3.2. Sample preparation*

Key to manufacturing CFRP-AA joints by UAM is to embed carbon fiber tows in the AA matrix, creating internal mechanical interlocking between the dissimilar materials. Figure 3 shows schematics of the manufacturing process.

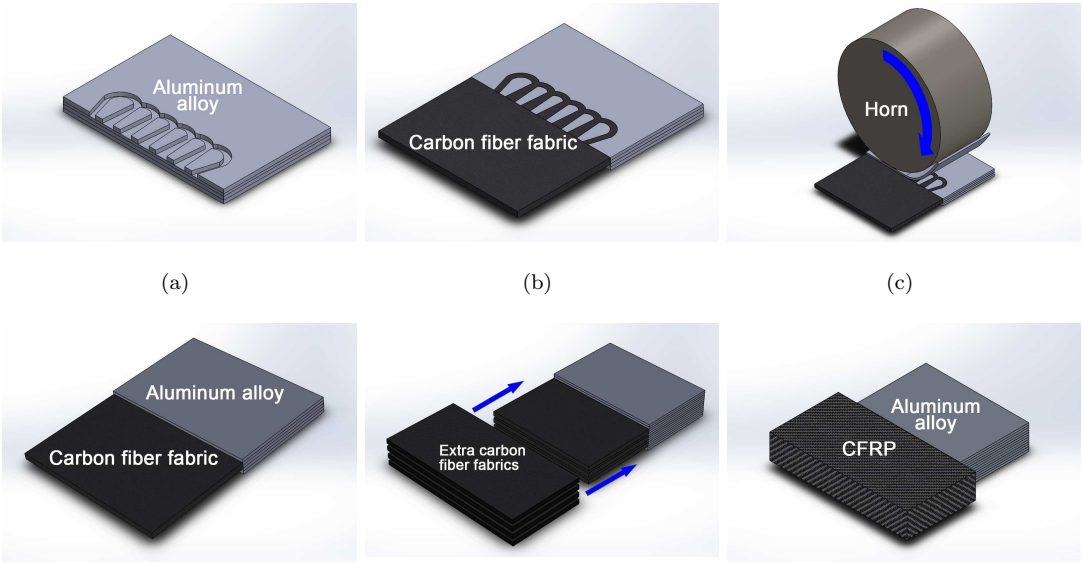


Figure 3: CFRP-AA joint manufacturing process: (a) AA matrix is built with UAM and channels are machined; (b) dry CF tow loops are placed in the channels; (c) one layer of AA foil is welded by the UAM horn; (d) one layer of CF tow loops is embedded; (e) three layers of CF tows are embedded by repeating steps (a) to (d), extra CF fabrics are inserted to match the thickness of CFRP to AA; (f) CFRP is cured with epoxy to complete the CFRP-AA joint.

The CF tows are encapsulated in n-shaped channels, as shown in Figure 4, with dimensions that correspond to the weft loops at the edge of the CF tape. The channel depth determines how compacted the fibers become during embedding. If the channels are over-filled, the fibers may not stay in the channel during welding or tearing of the foil being welded may occur. Considering these factors, the design shown in Figure 4 has deeper channels where neighboring CF tows overlap to accommodate the increased volume of carbon fibers. In the schematic, the darkness of the grey shading indicates the depth of the channel. The depth increases linearly from 0.18 mm to 0.36 mm to accommodate the transition from one to two CF tows.

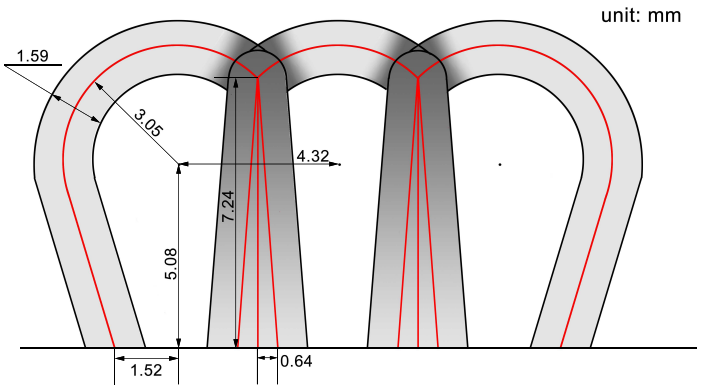


Figure 4: Schematic of looped channels to house the dry CF tows.

In this study, UAM transition joint coupons are fabricated with several layers of carbon fiber fabric embedded into an AA 6061 matrix. Side view schematics of two sample constructions for tensile testing are illustrated in Figure 5 (a) and (b). For the 3-CF-layer sample, there are 12 layers of AA 6061 foils, 3 embedded plies of CF fabric, and 4 layers of non-embedded CF fabric to preserve sample thickness. The 4-CF-layer sample has 4 layers of CF loops embedded into the AA matrix, which is made from 15 foil layers and 5 layers of non-embedded CF fabric. The thickness of the AA is 1.8 mm and 2.2 mm for the 3 and 4-CF layer builds, respectively.

The manufacturing process is illustrated in Figure 6. A section of the CF foil is cut out and some of the longitudinal tows that make up the warp of the fabric are removed to expose CF weft loops. To ensure that the tows are well situated in the channels and to avoid any drifting during the welding process, a light coating of spray adhesive is applied to the tows before placing them in the channels. An AA 6061 sheet is welded over the channels containing the tows [24]. Rather than using an automatically-fed AA 6061 tape foil, a layer of AA 6061-H18 sheet foil is secured over the sample with vacuum. The thickness of the AA sheet is the same as the typical AA tape foil used in UAM, though the sheet material is wider and can be trimmed to size as required to cover the sample. After a weld pass, the extra sheet material is removed from the sample. Following the sheet layer, several layers of AA 6061 tape foil are added to build up sufficient height for cutting additional channels and embedding more layers of CF fabric. After the welding process, a vent hole is drilled at the top of each loop to allow air to escape during vacuum bagging and ensure that the epoxy can fully wet the embedded CF loops. After the baseplate is removed using subtractive milling operations on the UAM system, the transition joint is laid up with additional CF fabric plies in between and on the outside of the embedded layers using epoxy. Samples 25.4 mm wide are cut from the final build for tensile testing.

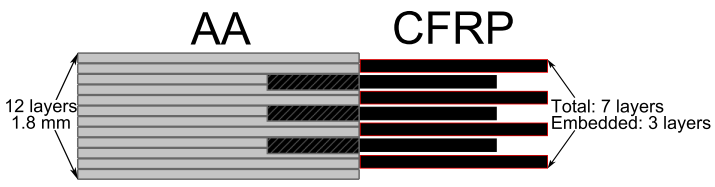


(a)

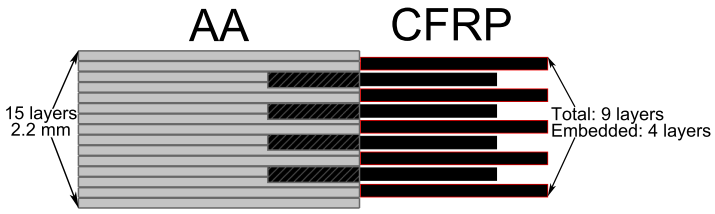


(b)

Figure 5: (a) Schematic cross section of 3-CF-layer transition joints; and (b) schematic cross section of 4-CF-layer transition joints. The CFRP component shown represents the CF after layup and cure in epoxy. (Schematics not drawn to scale.)

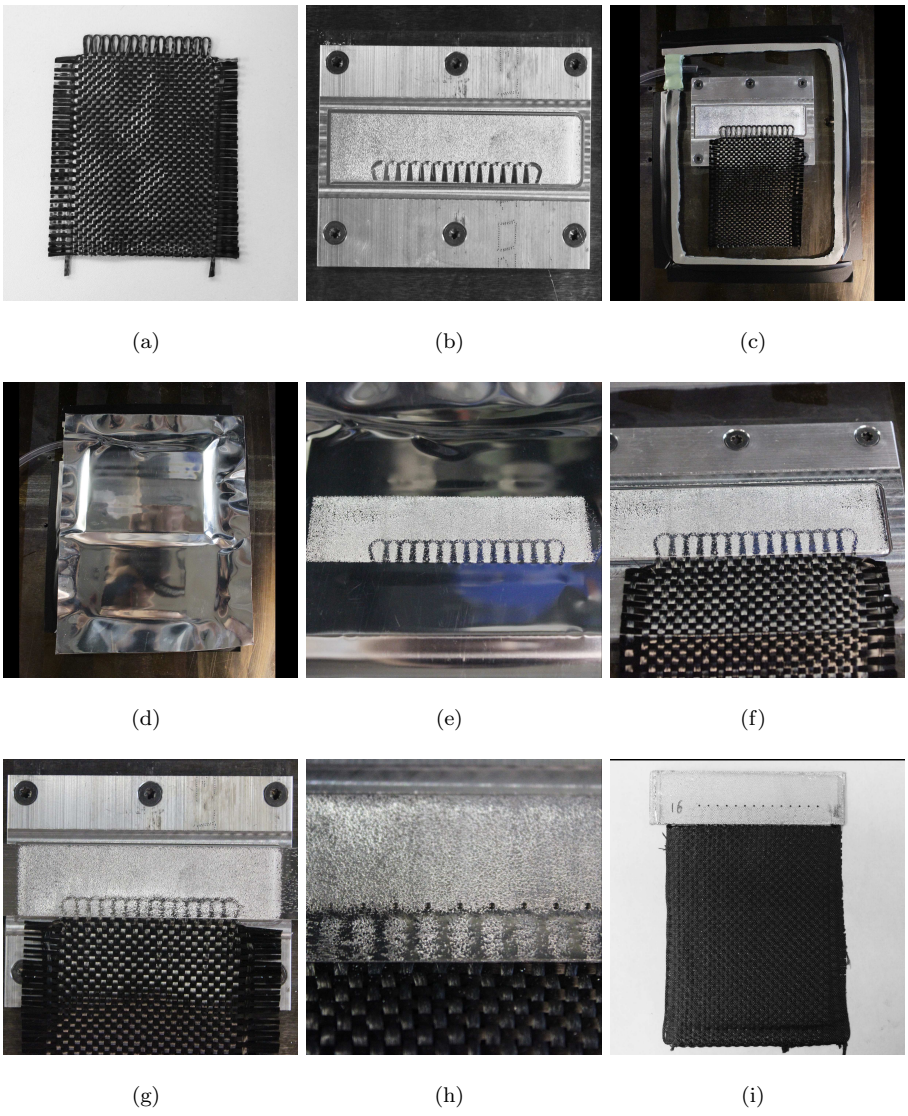

Figure 6: CFRP-AA transition joint manufacturing progression: (a) CF fabric is prepared by removing multiple warp tows; (b) four layers of AA 6061 tape foil are welded on the baseplate and the channels are cut into the AA matrix; (c) CF loops are placed into the channels with the aid of spray adhesive. Vacuum putty is set up around the sample with a vacuum hose passing through; (d) a layer of cleaned AA 6061 sheet foil is placed on the sample and secured by vacuum; (e) the AA 6061 sheet foil is welded over the CF tows using UAM; (f) extra sheet material is removed; (g) additional AA 6061 foils are welded over the base aluminum; (h) vent holes are drilled at the top of each loop; (i) additional CF fabrics are inserted into the CF part, and the joint is cured with epoxy in a vacuum bag at room temperature.

The parameters used to weld AA 6061-H18 are listed in Table 2. The welding parameters for tape

Table 2: Welding parameters for AA 6061-H18.

| | Force | Amplitude | Speed | Dwell time |
|---|---|---|---|---|
| AA 6061-H18 sheet foil | 4000 N | 30 $\mu$m | 80 in/min | 150 ms |
| AA 6061-H18 tape foil | 4000 N | 32 $\mu$m | 200 in/min | 300 ms |

foils follow the optimization result from a design of experiments (DOE) study carried out by Wolcott et al. [25]. A lower amplitude is used for sheet welding to avoid foil tearing or nuggeting. To compensate for the decrease in energy input, a lower welding speed is employed. This parameter set is typical for aluminum-to-aluminum UAM sheet welding.

### *3.3. Mechanical testing*

For measuring mechanical performance, tensile tests were conducted on 25.4 mm wide samples, shown in Figure 7. The tests were carried out on an MTS C43-504 load frame at a crosshead speed of 5 mm/min. During the tests, a Correlated Solutions VIC-3D Digital Image Correlation (DIC) system was used to evaluate the strain distribution and measure the local displacement in the joint area. A 20-mm virtual gage length across the joint region was used for measuring displacement. A force vs. displacement curve was plotted based on force data from the frame's load cell and the local displacement data measured by the DIC system.

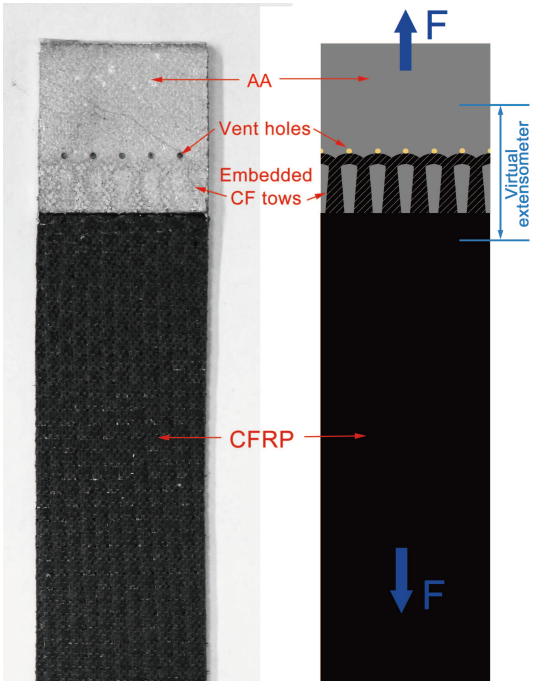


(a) (b)

Figure 7: CFRP-AA tensile samples: (a) picture and (b) schematic.

## 4. Optical imaging

Optical images of the hybrid joint were taken from a 3-CF layer sample to investigate the interface between an embedded CF tow and the AA matrix. Figure 8 shows two typical CFRP-AA interface characteristics at the channel side walls. The channels that accommodate the CF tows are slightly oversized in order to preserve tow integrity. In some regions, the CF tow is compactly encapsulated by the AA matrix, as shown in Figure 8 (b). It is also possible for the CF tow not to completely fill the channel, which leaves a space between the CF tow and the channel wall. However, when the sample is cured with epoxy, the vent holes ensure that the epoxy flows into the channel and completely fills the spaces, as pictured in Figure 8 (c). Oversizing the AA channels does not appear to harm the performance of the joint. On the contrary, the oversized channel design not only protects the CF tows from any damage due to welding, but also gives the epoxy the space needed to flow and consolidate the CF tows. It is emphasized that the primary role of epoxy in the channels is not to provide adhesion between the CF and AA since strength is provided by mechanical interlocking of the fiber loops in the matrix. Rather, consolidation of the tow provides load sharing between fibers to promote concurrent failure, thus improving strength. The epoxy present in the joint also helps to promote failure at two locations for each loop rather than just one failure point at the top of each loop during tensile testing,

which is the typical failure mode when dry fibers are pulled around a pillar or rod.

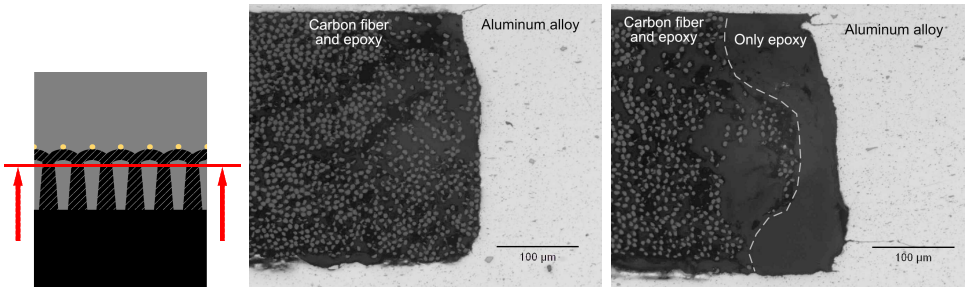


(a) (b) (c)

Figure 8: CFRP-AA interface at the channel side walls: (a) cross-section imaging location; (b) channel tightly packed with CF; and (c) channel that is not completely filled by CF where epoxy has flowed to fill the space between the CF and AA during layup.

Images of the CFRP-AA interface in Figure 9 show the difference between the upper and lower edges of the CF tow. Because the normal force applied during the welding process squeezes the CFs in the channel, some CF fibers are pushed into the AA matrix.

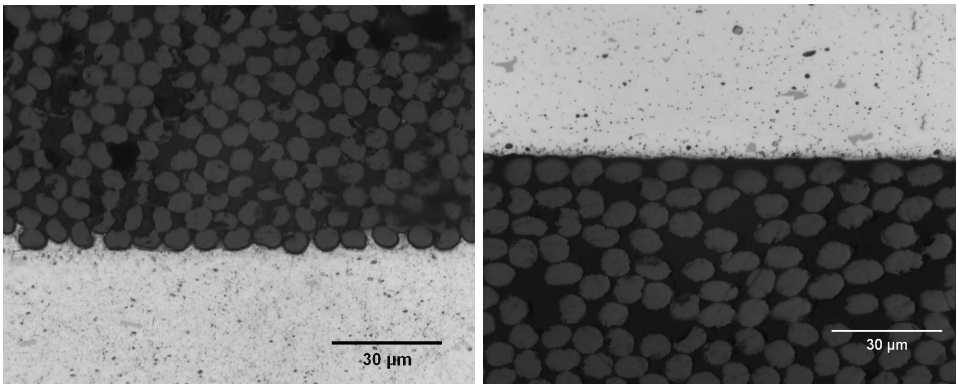


(a) (b)

Figure 9: CFRP-AA interface at the (a) lower edge and (b) upper edge.

## 5. Mechanical testing results

Tensile tests were conducted on 25.4 mm wide UAM CFRP-AA transition joint samples (3-CF-layer and 4-CF-layer) at a crosshead speed of 5 mm/min. The load vs. displacement curves are plotted in Figure 10. Because the sampling frequency of the DIC cameras is only 4 Hz, undersampling occurs as evidenced by the straight lines in the 3-CF-layer curves. The average peak load of the 3-CF-layer

samples is 4677 N while the average peak load of the 4-CF-layer samples reaches 7238 N. Two failure modes are observed. The 3-CF-layer samples fail in the CF tows and the 4-CF-layer samples fail in AA matrix. The average energy absorbed by the 3-CF-layer samples is 3.96 J, which is 4 times greater than the 0.9 J absorbed by the 4-CF-layer samples. The strain distributions and images of tested specimens will be illustrated and discussed for each failure mode.

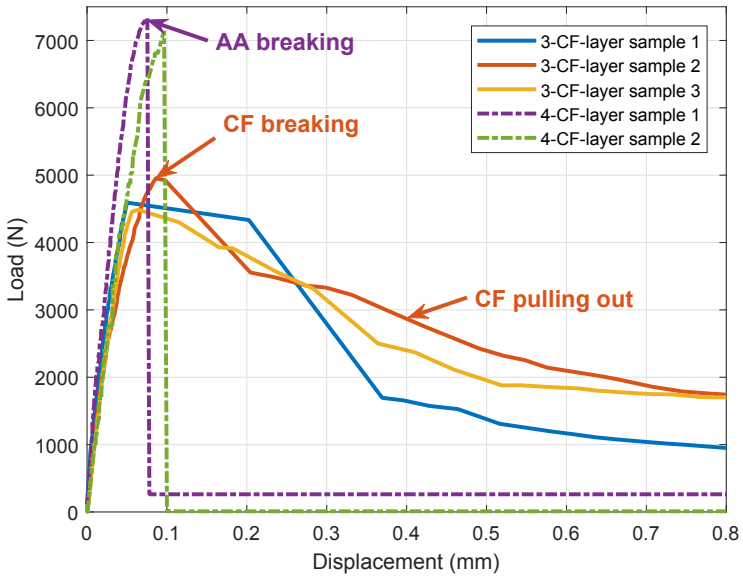


Figure 10: Load vs. displacement curves for tensile tests on 3-CF-layer and 4-CF-layer samples. The straight lines are caused by undersampling of the DIC system's cameras.

### *5.1. CF tow failure*

CF tow failure is the failure mode observed in the tensile testing of all 3-CF-layer UAM joints. Embedded carbon fiber loops break within the straight region of the channel loop, leaving the curved parts in the AA matrix. This failure mode is characterized by the CF tow loops breaking at two locations. The average peak tensile load for this sample design is 4677 N. Considering the joint's cross sectional area, the tensile strength is 102.3 MPa. As shown in Figure 10, the highest peaks in the 3-CF-layer load vs. displacement curves correspond to the CF breaking point, and the tail after the peak load is from friction during fiber pullout. The energy absorption of this failure mode is high due to the friction pullout. From the DIC strain map shown in Figure 11, the strain is evenly distributed at the beginning; as the load builds, the strain concentrates at the CFRP-AA interface as shown in Figure 11 (c). The CF tows carry load by pulling on the AA columns around which they are looped. The aluminum to CFRP tab interface breaks when the local true strain reaches 2%. As the load reaches a maximum value, the carbon fiber loops break and are pulled out after failure, shown in Figure 11 (d).

200 This CF pullout process contributes to the high energy absorption (3.96 J at 0.8 mm displacement). From the pictures of a failed sample shown in Figure 12, there is no delamination or AA shearing, which indicates that the UAM weld quality is high enough to avoid failure of the UAM weld in tensile testing.

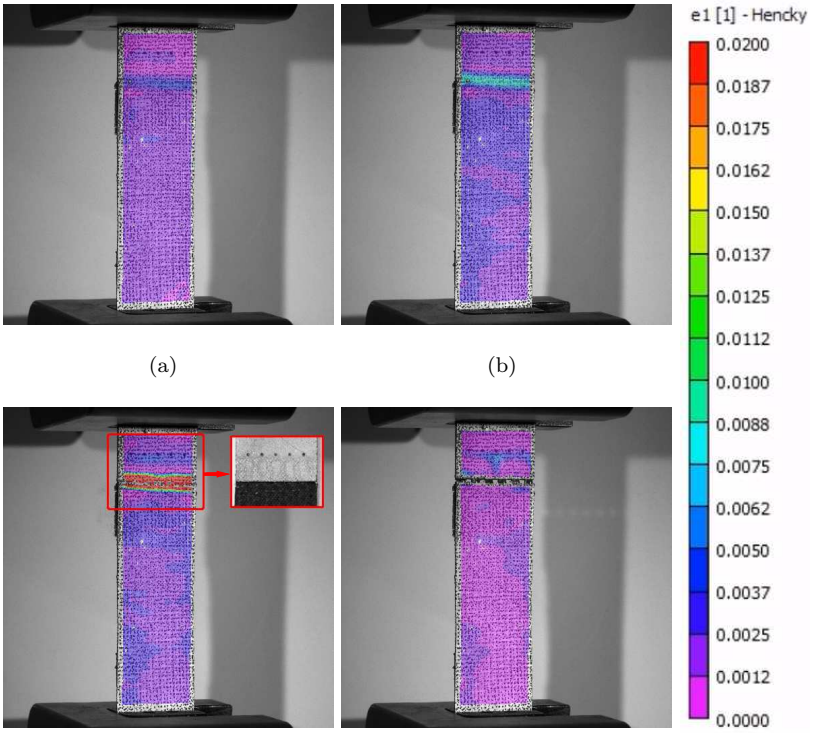


Figure 11: DIC strain maps at different displacements for 3-CF-layer sample 2: (a) 0.036 mm; (b) 0.057 mm; (c) 0.086 mm; and (d) 1.44 mm of displacement. Failure takes place in the CF tows.

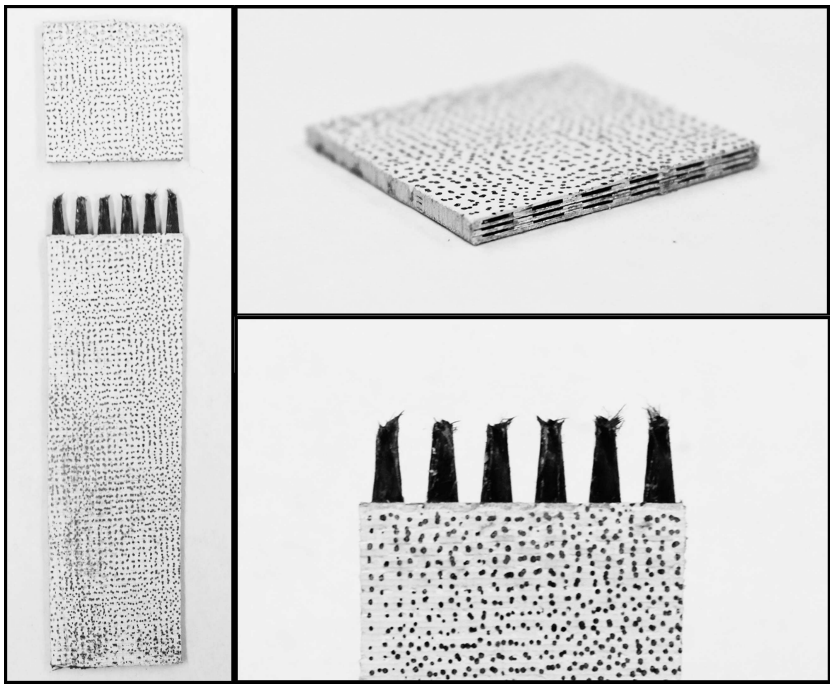

Figure 12: 3-CF-layer sample after tensile testing (speckled for DIC measurements).

In these samples, the CF tows are the weaker component when compared to the AA matrix. As illustrated in Figure 13, there are 10 CF tows per CF layer that carry load in a 25.4 mm wide sample. According to the single CFRP tow tensile test mentioned earlier, the peak load of each 3K CF tow is 200 N on average. Assuming the load is distributed uniformly among the CF tows, a 25.4 mm wide, 3-CF-layer CFRP-AA joint with 30 CF tows should be able to carry 6000 N. Referring to Figure 10, the difference between this calculation and the observed failure load may be explained by: (1) broken fibers observed in the CF tow loops of the as-received woven tape, which decreases the number of load-carrying CF fibers in each tow; and (2) nonuniform loading of CF tows leading to asynchronous failure of the carbon fibers. These two factors reduced the load carrying capacity of the 30 loaded CF tows by 1323 N, on average.

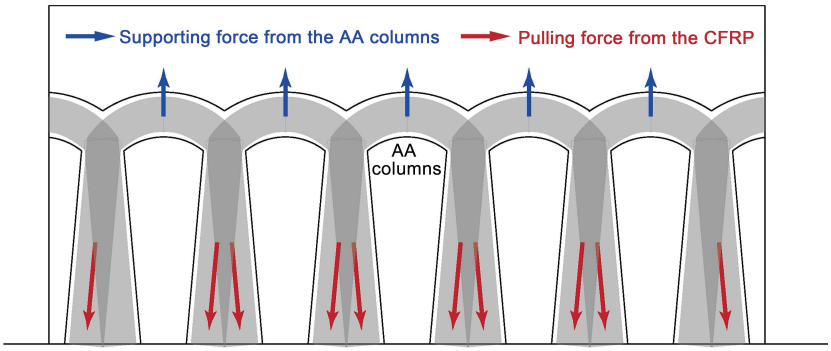


Figure 13: Loading diagram of one layer of CF loops in a 25.4 mm wide sample.

### *5.2. AA matrix failure*

The 4-CF-layer builds failed by breaking of the AA matrix. Analysis of the fracture surfaces (Figure 14) shows that the CFRP-AA joint interface was intact while the AA matrix failed in the stress concentration directly above the channel loops. This suggests that the UAM CFRP-AA joint is stronger than the AA matrix. The vent holes shown by the arrow are filled with epoxy; because epoxy is applied to the dry fabric outside of the UAM region before vacuum bagging, this indicates that the channels that house the CF tows are completely wetted. From the DIC strain map shown in Figure 15, the strain initially concentrates at the interfacial CFRP-AA area from the right side of the joint, shown in Figure 15 (b). As strain at the interface increases, severe strain concentration occurs at the top-of-loops region indicated in Figure 15 (c). Finally, the AA matrix cracked along the top edge of the loops when the strain of the AA matrix at the top-of-loops region reached 0.6%, leading to aluminum matrix failure shown in Figure 15 (d). The average peak load for the samples is 7238 N, which corresponds to a stress of 129.5 MPa. The only peak in the load vs. displacement curve in Figure 10 corresponds to failure of the AA matrix. The load drops to zero after this peak because the sample failed outside of the joint region, resulting in no fiber pullout.

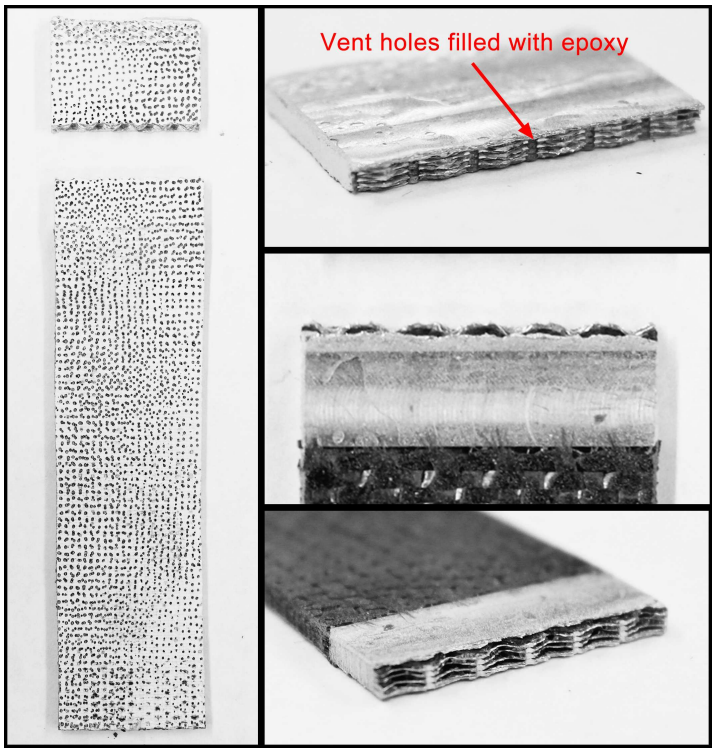


Figure 14: 4-CF-layer sample after testing (speckled for DIC measurements).

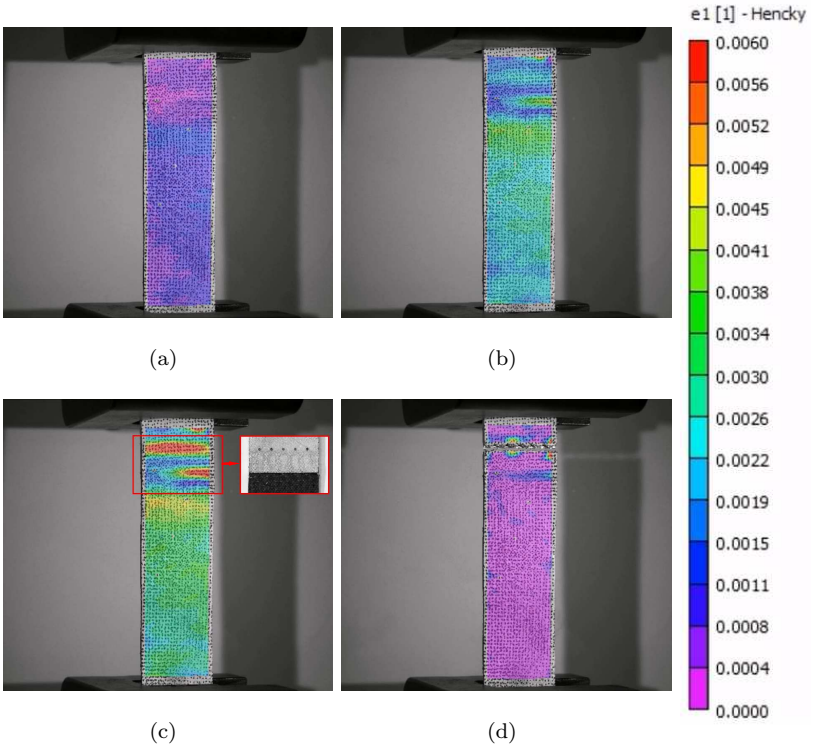


Figure 15: DIC strain maps at different displacements for a 4-CF-layer sample failing in the AA matrix: (a) 0.011 mm; (b) 0.045 mm; (c) 0.076 mm; and (d) 2.13 mm.

The schematic of the projection perpendicular to the loading direction of the surface along the AA failure interface is shown in Figure 16. The projected area of the AA matrix along the failure interface is 36.06 $mm^2$. Since the UTS of the AA matrix (UAM welded AA 6061-H18) is 195 MPa, the theoretical peak load of this failure mode is 7032 N. The difference between experimental and theoretical peak loads may be caused by the adhesive strength of the epoxy at the end of the CFRP tows and vent holes.

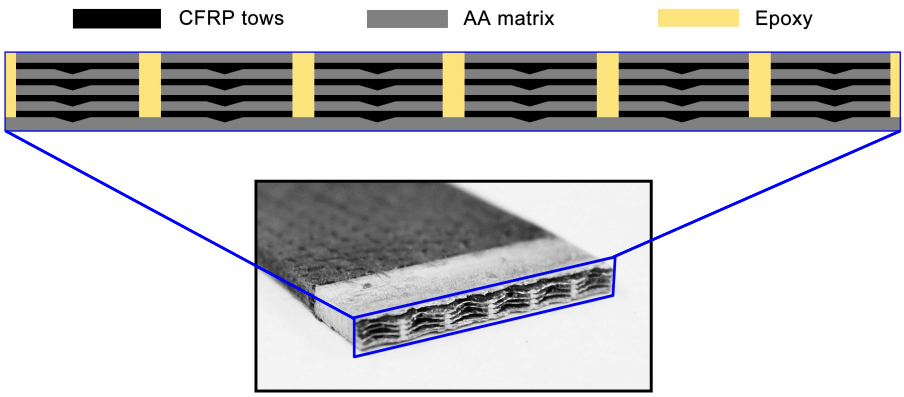


Figure 16: Schematic of the projection of an AA failure interface.

## 6. Summary

Ultrasonic additive manufacturing was applied to create joints between AA 6061 and CFRP by mechanical interlocking, producing a high strength joint with distinct features relative to existing techniques. One feature is the designable failure mode. Samples with 3 layers and 4 layers of CF were built and mechanically tested. Tensile tests show that the peak loads for 1.8 mm thick 3-CF-layer samples and the 2.2 mm thick 4-CF-layer sample are 4677 N and 7238 N, respectively. The failure modes of both sample geometries were analyzed by strain distribution maps recorded through DIC. Failure mechanism analyses on both sample constructions demonstrate that the failure mode, i.e., CF tow failure or AA matrix failure, can be designed by tuning the CF/AA ratio. The ideal failure mode for CFRP-AA joints may vary in different situations. Since UAM is an additive manufacturing process, the failure mode of the joints can be designed by simply adjusting the number of AA and CF layers. For example, if the thicknesses of the aluminum and CFRP parts are given, a larger number of embedded CF layers will result in AA failure, providing an efficient joint in terms of specific strength and stiffness, while a CF failure mode can be created by embedding fewer CF tows, resulting in higher energy absorption. This ability to change the CF:AA ratio to achieve a predicted performance outcome is an important feature of the UAM CFRP-AA joint. Another special characteristic of the UAM CFRP-AA joint is that it maintains the thickness of the aluminum part across the joint; the joints require no overlaps and associated discontinuities. The looped channel geometry makes it possible to create a continuous joint between CF and aluminum with any arbitrary interface profile. With the approach presented here, metal tabs can be added to CFRP parts for subsequent welding of these parts to metal structure via resistance spot welding. The ability to integrate CFRP parts and metal structures without requiring changes to existing metal welding infrastructure is regarded as a major

benefit of the approach presented here. Although this study focused on Al-CF transitions, this design can be optimized for other metal-fiber combinations.

## References


[1] S. B. Shea, 54.5 MPG and Beyond: Materials Lighten the Load for Fuel Economy, 2012. https://www.energy.gov/articles/545-mpg-and-beyond-materials-lighten-load-fuel-economy.

[2] W. J. Joost, Reducing vehicle weight and improving U.S. energy efficiency using integrated computational materials engineering, JOM 64 (2012) 1032–1038.

[3] M. F. Ashby, D. Cebon, Materials selection in mechanical design, Le Journal de Physique IV 3 (1993) C7–1.

[4] T. Barnes, I. Pashby, Joining techniques for aluminium spaceframes used in automobiles Part II — adhesive bonding and mechanical fasteners, Journal of Materials Processing Technology 99 (2000) 72–79.

[5] J. M. Arenas, C. Alía, J. J. Narbón, R. Ocaña, C. González, Considerations for the industrial application of structural adhesive joints in the aluminium–composite material bonding, Composites: Part B 44(1) (2012) 417–423.

[6] T. Ribeiro, R. Campilho, L. Da Silva, L. Goglio, Damage analysis of composite-aluminium adhesively-bonded single-lap joints, Composite Structures 136 (2016) 25–33.

[7] G. Marannano, B. Zuccarello, Numerical experimental analysis of hybrid double lap aluminum-CFRP joints, Composites: Part B 71 (2014) 28–39.

[8] F. Lambiase, D.-C. Ko, Two-steps clinching of aluminum and carbon fiber reinforced polymer sheets, Composite Structures 164 (2017) 180–188.

[9] Y. Zhai, D. Li, X. Li, L. Wang, An experimental study on the effect of joining interface condition on bearing response of single-lap, countersunk composite-aluminum bolted joints, Composite Structures 134 (2015) 190–198.

[10] F. Balle, G. Wagner, D. Eifler, Ultrasonic spot welding of aluminum sheet/carbon fiber reinforced polymer – joints, Materialwissenschaft und Werkstofftechnik 38 (2007) 934–938.

[11] F. Lionetto, F. Balle, A. Maffezzolia, Hybrid ultrasonic spot welding of aluminum to carbon fiber reinforced epoxy composites, Journal of Materials Processing Tech. 247 (2017) 289–295.

[12] K. Nagatsuka, S. Yoshida, A. Tsuchiya, K. Nakata, Direct joining of carbon-fiber–reinforced plastic to an aluminum alloy using friction lap joining, Composites: Part B 73 (2014) 82–88.

[13] N. M. André, S. M. Goushegir, J. F. dos Santos, L. B. Canto, S. T. Amancio-Filho, Friction spot joining of aluminum alloy 2024-T3 and carbon-fiber-reinforced poly(phenylene sulfide) laminate with additional PPS film interlayer: microstructure, mechanical strength and failure mechanisms, Composites: Part B 94 (2016) 197–208.

[14] S. Goushegir, J. dos Santos, S. Amancio-Filho, Influence of aluminum surface pre-treatments on the bonding mechanisms and mechanical performance of metal-composite single-lap joints, Welding in the World 61 (2017) 1099–1115.

[15] P. Mitschang, R. Velthuis, M. Didi, Induction spot welding of metal/CFRPC hybrid joints, Advanced Engineering Materials 15 (2012) 804–813.

[16] A. Zajkani, M. Salamati, Numerical and experimental investigation of joining aluminium and carbon fiber reinforced composites by electromagnetic forming process, in: 7th International Conference on High Speed Forming, Dortmund, 2016, pp. 59–68.

[17] P. J. Wolcott, M. J. Dapino, Ultrasonic additive manufacturing, in: A. Badiru, V. Valencia, D. Liu (Eds.), Additive Manufacturing Handbook: Product Development for the Defense Industry, CRC Press/Taylor and Francis, Boca Raton, Florida, 2017.

[18] C. Kong, R. Soar, P. Dickens, Optimum process parameters for ultrasonic consolidation of 3003 aluminium, Journal of Materials Processing Technology 146 (2003) 181–187.

[19] R. Hahnlen, M. J. Dapino, Stress-induced tuning of ultrasonic additive manufacturing Al-NiTi composites, in: Behavior and Mechanics of Multifunctional Materials and Composites 2012, volume 8342, SPIE, San Diego, 2012. doi:10.1117/12.915582.

[20] R. Hahnlen, M. J. Dapino, NiTi-Al interface strength in ultrasonic additive manufacturing composites, Composites: Part B 59 (2013) 101–108.

[21] A. Hehr, M. J. Dapino, Interfacial shear strength estimates of NiTi–Al matrix composites fabricated via ultrasonic additive manufacturing, Composites Part B: Engineering 77 (2015) 199–208.

[22] J. J. Schomer, A. J. Hehr, M. J. Dapino, Characterization of embedded fiber optic strain sensors into metallic structures via ultrasonic additive manufacturing, in: Sensors and Smart Structures Technologies for Civil, Mechanical, and Aerospace Systems, volume 9803, SPIE, Las Vegas, 2017. doi:10.1117/12.2219690.

[23] P. J. Wolcott, C. Pawlowski, L. M. Headings, M. J. Dapino, Seam welding of aluminum sheet using ultrasonic additive manufacturing system, Journal of Manufacturing Science and Engineering 139 (2016) 011010.

[24] J. Wenning, Fabrisonic LLC, personal communication, May 18 2017. .

[25] P. J. Wolcott, A. Hehr, M. J. Dapino, Optimized welding parameters for Al 6061 ultrasonic additive manufactured structures, Journal of Materials Research 29 (2014) 2055–2065.